

Neutronics Studies for a Long-Wavelength Target Station at SNS

B. J. Micklich^a, E. B. Iverson^b, and J. M. Carpenter^c

^a*Technology Development Division, Argonne National Laboratory, Argonne, IL 60439*

^b*Spallation Neutron Source, Oak Ridge National Laboratory, Oak Ridge, TN 37831*

^c*Intense Pulsed Neutron Source, Argonne National Laboratory, Argonne, IL 60439*

Abstract. The Spallation Neutron Source (SNS), under construction at Oak Ridge National Laboratory, will be the premier facility for neutron scattering studies in the United States. From the outset the SNS can achieve additional flexibility and accommodate a broader range of scientific investigation than would be possible with only the High Power Target Station by utilizing two target stations, each operating under a separate set of conditions and optimized for a certain class of instruments. A second target station, termed the Long-Wavelength Target Station (LWTS), would operate at a lower pulse rate (e.g., 10 vs. 60 Hz) and utilize very cold moderators to emphasize low-energy (long wavelength) neutrons. The LWTS concept discussed here obtains the highest low-energy fluxes possible for neutron scattering instruments by using a heavy-water-cooled solid tungsten target with two moderators in slab geometry and one in a front wing position. The primary focus has been on solid methane moderators, with liquid methane and hydrogen also considered. We used MCNPX to conduct a series of optimization and sensitivity studies to help determine the optimal neutronic parameters of the LWTS. We compared different options based on the thermal and epithermal fluxes as determined by fitting the spectral intensity of the moderators with a Maxwellian peak and a modified Westcott function. The primary parameters are the moderator positions and composition and the target size. We report results for spectral intensity, pulse shapes, high-energy neutron emission, heating profiles in the target, and target activation.

1. INTRODUCTION

The Spallation Neutron Source (SNS) project has always planned that two target stations would eventually be built at the SNS facility, although only one is funded under the current project. Having two target stations, each operating under a separate set of conditions and optimized for a certain class of instruments, would permit greater flexibility in design and accommodate a broader range of scientific investigation. The High Power Target Station (HPTS) will offer both ambient-temperature and cryogenic moderators, designed to deliver the highest-intensity beams for applications that can exploit the 60-Hz pulsing frequency. The proposed Long Wavelength Target Station (LWTS) will operate at 10 Hz, allowing a broader spectrum of neutrons to be used while simultaneously permitting the use of colder, more efficient moderators for producing long-wavelength

neutrons. Optimization for long-wavelength neutrons implies extensive implementation of curved guides and compact beam benders, which in turn enables use of tall slab moderators. Discussion of the philosophy of the design effort may be found elsewhere.[1] Herein we describe neutronics design studies for the LWTS effort.

Section 2 describes the neutronically relevant aspects of the LWTS, Sec. 3 presents some of the performance characteristics of the current LWTS concept, and Sec. 4 outlines some sensitivity studies performed as part of the design process. We discuss high-energy neutron aspects of the LWTS design in Sec. 5, and target heating and activation in Sec. 6.

2. LWTS CONFIGURATION

The Monte Carlo radiation transport code MCNPX, version 2.1.5 [2] was used to calculate the neutron beam characteristics (moderator performance) and thermal power generation in the target and moderator systems. While MCNPX is still considered a beta-release code, it is based on the codes LAHET [2] and MCNP [3], well-accepted standard codes for this type of analysis. MCNPX has the advantage that it calculates both the high-energy ($E > 20$ MeV) and the lower energy ($E < 20$ MeV) portions of the problem for all particles together. We used the Bertini intranuclear cascade model, which is currently the most widely-accepted model available in production-class codes for particle energies less than 3 GeV, and no pre-equilibrium particle emission (since we found no difference in results with that feature turned on).

MCNPX employs a combinatorial geometry that represents the physical system using generalized quadratic surfaces to define the boundaries of cells. The modeled system is somewhat simpler than the actual design of the target station. For example, the model does not include coolant pipes for moderators and approximates the multiplicity of nested vessels surrounding the moderators as single homogenized volumes. However, the model provides sufficient detail to obtain adequate estimates for quantities such as neutron beam characteristics of the moderators and the energy deposition in the moderators and target.

2.1 LWTS Neutronics Model Description

The LWTS reference concept includes a vertically extended target of clad tungsten metal plates cooled with D_2O . The plates measure 7 cm wide \times 20 cm high and have variable thickness, with a total length of 40 cm. The shape of the target maximizes neutron production and coupling to the moderators while minimizing proton leakage to the surroundings. The target length exhausts the nuclear cascade and leaves little power to be deposited in the downstream shielding. The nominal proton beam power is 1/3 MW corresponding to 10-Hz operation.

The incident proton beam has an energy of 1 GeV. Its footprint is a 5-cm \times 15-cm elliptical shape with a flat distribution, similar to that for the HPTS. The two-dimensional beam current density profile (see Fig. 1) is represented in terms of an error function

$$\rho(r) = \frac{1}{2} \left[1 + \operatorname{erf} \left(\frac{r_0 - r}{a} \right) \right] \quad r < r_0$$

$$= \frac{1}{2} \operatorname{erfc} \left(\frac{r - r_0}{a} \right) \quad r > r_0,$$

where $r_0 = \sqrt{x_0^2 + y_0^2}$, x_0 and y_0 are defined by the ellipse $(x_0/7.5)^2 + (y_0/2.5)^2 = 1$, and $a = 1.52 \cdot (r_0/7.5)$ [chosen so that $\rho = 0.01$ at the top edge of the target plate]. Some early calculations used a vertically extended rectangular beam of cross section 5 \times 14 cm or 7 \times 20 cm.

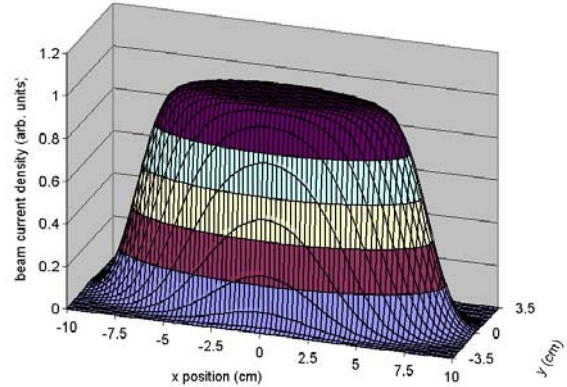


FIG. 1. Proton beam profile used for neutronics analysis of LWTS.

The reference LWTS model (Fig. 2) contains three moderators adjacent to the neutron producing target. Two moderators are in “slab” geometry (spallation neutron source behind the viewed surface) and one is in a “wing” position (source not behind the viewed surface) upstream of the target. The High-Intensity Cold Moderator is the slab moderator to the left of the target when viewed from the perspective of the incident proton beam. It is fully coupled to the reflector. The viewed surface of the moderator has horizontal V-shaped grooves with an opening angle of 30° . The moderating material is either solid methane at 22 K (90% by volume) and aluminum (10% by volume) or liquid hydrogen at 20 K. Each moderator material has its own particular advantages, and the choice between the two materials will have to be made based on the needs of instruments that will view the moderator. The High-Resolution Cold Moderator is to the right of the target when viewed from the perspective of the incident proton beam. It is composed of solid methane at 22 K (90% by volume) and aluminum (10% by volume), decoupled from the reflector with cadmium and poisoned with gadolinium at a depth of 2.5 cm beneath the viewed surface. The High-Resolution Broadband Moderator is on the right side, just upstream of the proton beam target. It

consists of either liquid methane at 100 K or the methane-aluminum mixture at 22 K, decoupled with cadmium and poisoned with gadolinium at a depth of 2.5 cm beneath the viewed surface. We present results for all these choices of moderator materials. Table I summarizes the important neutronics parameters of the LWTS reference model.

All three of the moderator materials considered have high hydrogen densities (L-H₂ to a somewhat lesser degree), which makes them very efficient moderators. By choice of overall thickness and poisoning depth, it is possible to tune each moderator to optimize the trade-offs between neutron pulse

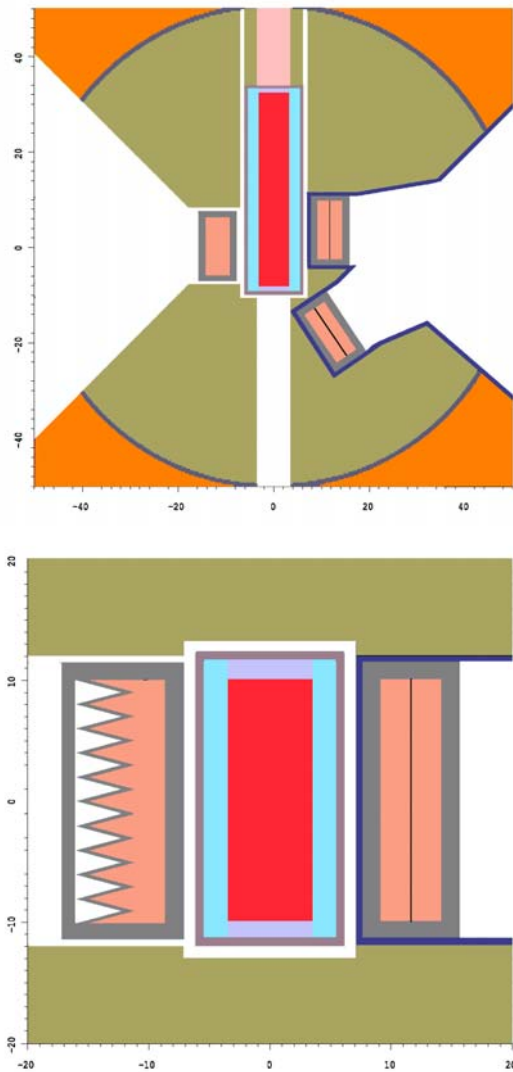


FIG. 2. MCNPX neutronics model for the reference LWTS target/reflector/moderator system (decouplers not to scale). Protons are incident from the bottom in the upper picture and into the page in the lower picture.

width, spectral temperature, and overall flux as appropriate for the instruments to which it supplies neutrons. We have not yet undertaken detailed optimizations of this type, so the performance values given herein could be improved upon but in any case provide a high standard of performance.

2.2 Quantities Calculated

The spectral intensity $i(E)$ of a moderator is a measure of the number of neutrons leaving the entire viewed face of the moderator at a particular energy E and is related to the differential flux $\phi(E)$ at a point some large distance L from the moderator by a “ $1/r^2$ ” relationship, that is,

$$i(E) = L^2 \phi(E)|_L, \quad (1)$$

where the flight path is normal to the viewed moderator face. This intensity characterizes the moderator independently of the flight path length from which it is viewed. If the flight path is not normal to the moderator face, the observed intensity is approximately proportional to the cosine of the angle between the flight path and the normal to the moderator surface (Lambert’s Law).

TABLE I. Geometrical and Material Features of the LWTS Neutronics Model.

Component	Material/Geometry/Dimensions
Target	tungsten plates, rectangular, 20 cm high x 7 cm wide
Housing	SS, rectangular, 0.6 cm thick
Coolant	D ₂ O, 0.1-cm channel gap between plates; 1 cm thick above and below target
Premoderator	H ₂ O, 2 cm thick region on target sides
Moderators	
High-Intensity Cold	solid methane or liquid hydrogen, 20 cm (h) x 12 cm (w) x 5 cm (t)
High-Resolution Cold	solid methane, 20 cm (h) x 12 cm (w) x 5 cm (t)
High-Resolution Broadband	liquid or solid methane, 20 cm (h) x 12 cm (w) x 5 cm (t)
Decoupler	Cadmium, 1 mm around moderators and neutron beamlines (except moderator faces)
Poison	Gadolinium, 50 μm thick
Reflector	D ₂ O-cooled Be, cylinder, 50 cm diameter x 100 cm high
Shield	Water-cooled Fe, radially to 6 m, vertically ± 4 m

The spectral intensities are calculated both by point detector tallies, which give rapid convergence, absolute scaling, and directional sensitivity, and by leakage current tallies, which provide intensities for high-energy neutrons (the way that the point detector tally works in MCNPX does not permit contributions from high-energy neutrons). The use of slab moderators requires careful examination of the high-energy neutron source term. Therefore we calculate the spectral intensities up to some 500 MeV using leakage current tallies, which we normalize using point detector results in an energy range where both tallies function properly.

The emission time distribution $i(E,t)$ of the moderator for a given neutron energy, also called the pulse shape, is the intensity distribution as a function of the time at which the neutrons cross the moderator surface. It is related to the spectral intensity by

$$i(E) = \int_0^{\infty} i(E,t) dt. \quad (2)$$

The emission time distribution of the neutrons leaving the moderator is presumed to depend on the viewing angle only in the scaling of the overall intensity. The energy and time bins in the MCNPX calculations provide 10 energy bins and 20 time bins per decade, such that $\Delta E/E \approx 23\%$ and $\Delta t/t \approx 11\%$. The results reported are differential values averaged over such bins. Emission time distributions are those calculated by surface-averaged leakage current tallies, normalized by point detector intensity tallies.

3. REFERENCE MODEL RESULTS

3.1 Neutron Spectra

The time-averaged neutron spectral intensity $E \cdot i(E)$ from a moderator at a pulsed source, the number of neutrons per steradian per unit lethargy per unit time, can be represented by a Maxwellian thermal spectrum joined to a nearly $1/E$ epithermal spectrum, which has the form of a modified Westcott spectrum

$$E \cdot i(E) = I_{th} \left[\frac{E^2}{E_t^2} e^{-E/E_t} \right] + I_{epi} \Delta(E) \left[\frac{E}{E_{ref}} \right]^\alpha. \quad (3)$$

In this equation, E_t is a characteristic energy of the Maxwellian portion of the spectrum; $\Delta(E)$ is a joining function, which goes smoothly from 0 (for E below

about $5E_t$) to 1 (for E above about $5E_t$); E_{ref} is a reference energy, typically taken to be 1 eV; and α is a constant, the ‘‘leakage exponent,’’ with a value about 0.05. I_{th} and I_{epi} are scaling constants for the thermal and epithermal portions of the spectrum, respectively. We use fits of this equation to the MCNPX output data to characterize the neutronic performance of the moderators and to investigate the effects of changes introduced into the models. For the coupled moderators, there is a significant thermal leakage component from the reflector that appears at all angles but most strongly at large angles to the surface normal. To account for this, we add an additional room-temperature thermal term to Eq. (3) corresponding to reflector-leakage neutrons. The coefficient for this term is generally much smaller than the moderator thermal term and is not reported in the following results.

Figure 3 shows the normally-emerging neutron spectral intensities for moderators in the reference geometry. For the coupled moderator, liquid hydrogen provides more total neutrons and a higher spectral intensity for neutron energies above 6 meV. Solid methane has an advantage as a coupled moderator for energies below 6 meV, an energy range that we believe to be of great interest for instruments on the LWTS. The front wing moderator using solid methane gives a thermal flux about 62% that of the decoupled slab, with the epithermal spectral intensity about 60% that achieved in the decoupled slab. With liquid methane in the front wing position, the moderator gives a thermal flux about 92% that of the solid methane decoupled slab, but at energies characteristic of the higher temperature material (i.e., the peak occurs at around 20 meV rather than at about 5 meV for the solid methane).

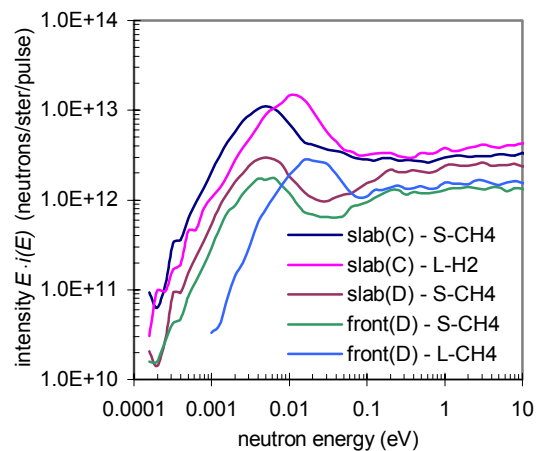


FIG. 3. Neutron spectral intensities for reference LWTS moderators.

3.2 Neutron Pulse Widths

The pulse shapes of neutrons emerging from a moderator are highly energy dependent but do not depend significantly on emission angle. The widths of these pulses can be changed dramatically by varying the poisoning and decoupling parameters and by varying the moderator material. The premoderator geometry may also have an effect. In general, for a given moderator material, the intensity varies roughly inversely with the square of the pulse width. Thus, there are a large number of degrees of freedom that can be varied to optimize moderators for the requirements of specific sets of instruments.

Figure 4 shows the energy-dependent pulse widths (FWHM) for the moderators we have considered in the reference model. In this figure, the FWHM for each moderator at each energy is that estimated by fitting the time dependence with a log-normal distribution. The flat (decoupled) methane moderators all have roughly the same pulse width for neutron energies above 0.1 eV, below which the liquid methane moderator exhibits a broader pulse. The grooved (coupled) solid methane moderator yields a broader pulse (twice the FWHM) than the flat solid methane moderators. The broader pulse is due to the grooved nature of the moderator; a flat coupled solid methane moderator would have the same pulse width as a decoupled one for neutron energies above 0.01 eV. Liquid hydrogen exhibits a significantly broader pulse than the decoupled moderators at all energies, which is compensated somewhat by its overall higher spectral intensity.

The FWHM values reported here are representative values only. The detailed pulse shapes

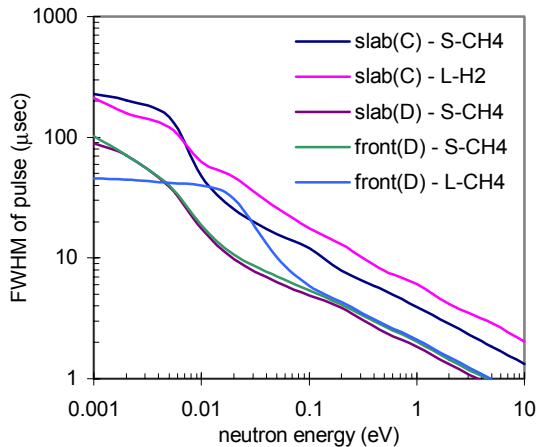


FIG. 4. Pulse width (FWHM) for LWTS reference moderators as a function of neutron energy.

will determine the performance of a given instrument. Small changes in the decoupling and/or poisoning can give rise to variations of a factor of 2 in I_{th} and to correspondingly large variations in the pulse width. Because of the great degree of tunability in moderator performance, moderator details will necessarily be the subject of extensive joint optimization with instrument design. Moreover, the proposed LWTS target/moderator/reflector arrangement would facilitate changing moderators at some future date.

4. SENSITIVITY STUDIES

We performed a large number of sensitivity studies to guide the target and moderator design process. Most of these had the objective of determining the effects of a single change around a point design and do not represent rigorous attempts to optimize any one or a set of design parameters. Taken as a whole, they point to the directions one should take in performing system optimizations. Results from several of these studies follow, while others may be found in an earlier publication [5].

4.1 Light-Water vs. Heavy-Water Coolant

Light water is generally selected as the target coolant because of its superior moderating properties. However, it does have a small but significant absorption cross section for thermal neutrons. Moderation within the target also increases thermal neutron capture in the target material. We investigated the effect of changing all the coolant in the vicinity of the target to heavy water except that between the target and the slab moderators, which serves as a premoderator. In general, the use of heavy water increases the thermal and epithermal spectral intensities by about 10% (see Table II). Therefore we have adopted heavy water coolant for the reference configuration.

4.2 Full-Size vs. Half-Size Target

Because the peak energy deposition rate in the 20-cm x 7-cm target plates is only about 250 W/cm³ (see Sec. 6), we performed a calculation in which the target and the beam profile were smaller by about a factor of 0.7 in each dimension, with the goal of increasing the peak energy deposition to about 500 W/cm³. We saw gains in neutronic performance for all three moderators, about 5% and 13% increase in thermal

neutron intensity for the decoupled and coupled moderators, respectively, as shown in Table III. Although the higher power density is probably tolerable, we have adopted the conditions that lead to the conservative 250 W/cm³.

TABLE II. Thermal (I_{th}) and epithermal (I_{epi}) spectral parameters for light- and heavy-water coolant.

	front wing (solid meth)	coupled slab (solid meth)	decoupl. slab (solid meth)
I_{th}			
H ₂ O	2.85e+12	1.01e+13	4.50e+12
D ₂ O	3.08e+12	1.11e+13	4.93e+12
change	+ 8.1 %	+ 9.9 %	+ 9.6 %
I_{epi}			
H ₂ O	1.42e+12	2.40e+12	2.30e+12
D ₂ O	1.53e+12	2.62e+12	2.55e+12
change	+ 7.8 %	+ 9.2 %	+ 11.0 %
	front wing (liquid meth)	coupled slab (LH2)	decoupl. slab (solid meth)
I_{th}			
H ₂ O	4.06e+12	2.55e+13	4.55e+12
D ₂ O	4.50e+12	2.66e+13	4.86e+12
change	+ 10.8 %	+ 4.3 %	+ 6.8 %
I_{epi}			
H ₂ O	1.43e+12	3.54e+12	2.32e+12
D ₂ O	1.59e+12	3.74e+12	2.63e+12
change	+ 11.2 %	+ 5.6 %	+ 13.4 %

TABLE III. Thermal (I_{th}) and epithermal (I_{epi}) spectral parameters for full-size and half-size target.

	front wing (solid meth)	coupled slab (solid meth)	decoupl. slab (solid meth)
I_{th}			
full size	2.85e+12	1.01e+13	4.50e+12
half size	3.00e+12	1.15e+13	4.72e+12
change	+ 5.3 %	+ 13.9 %	+ 4.9 %
I_{epi}			
full size	1.42e+12	2.40e+12	2.30e+12
half size	1.52e+12	2.63e+12	2.49e+12
change	+ 7.0 %	+ 9.6 %	+ 8.3 %
	front wing (liquid meth)	coupled slab (LH2)	decoupl. slab (solid meth)
I_{th}			
full size	4.06e+12	2.55e+13	4.55e+12
half size	4.27e+12	2.87e+13	4.84e+12
change	+ 5.2 %	+ 12.5 %	+ 6.4 %
I_{epi}			
full size	1.43e+12	3.54e+12	2.32e+12
half size	1.50e+12	3.80e+12	2.46e+12
change	+ 4.9 %	+ 7.3 %	+ 6.0 %

4.3 Flat vs. Grooved Moderator

An early reference design utilized flat viewed surfaces for both decoupled and coupled moderators. As part of our sensitivity studies, we compared the neutronic performance of the grooved moderator concept shown in Fig. 2 with that of the flat moderator shown in Fig. 5. The volume of moderator material in the grooved moderators is the same as in the flat moderators, but neither the grooved nor the flat moderator geometry was optimized for either of the moderator materials studied.

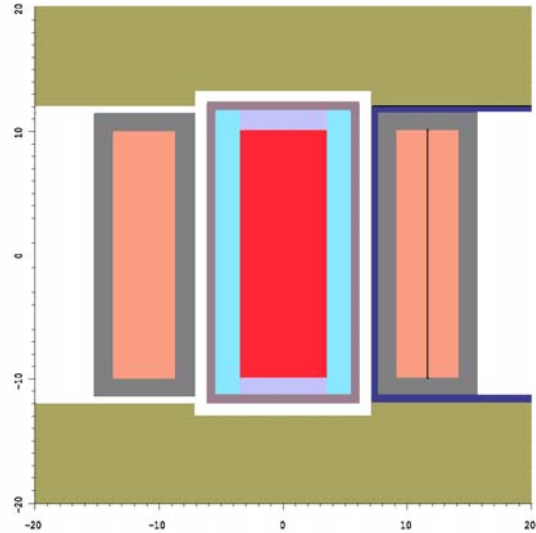


FIG. 5. MCNPX neutronics model of the LWTS geometry incorporating a coupled slab moderator with a flat viewed surface (decoupler not shown to scale).

Figure 6 shows the normally-emergent neutron spectral intensities for the flat and grooved moderators, for both solid methane and liquid hydrogen materials. For the solid methane, there is a clear improvement in the performance at all energies. For liquid hydrogen, the two moderator shapes have equivalent epithermal neutron intensities, but the grooved moderator has lowered performance for thermal energies. We believe this is because the liquid hydrogen, having a lower hydrogen density than solid methane, is optically thinner at these energies. However, an optimized moderator design for liquid hydrogen would likely yield an improvement over the flat moderator.

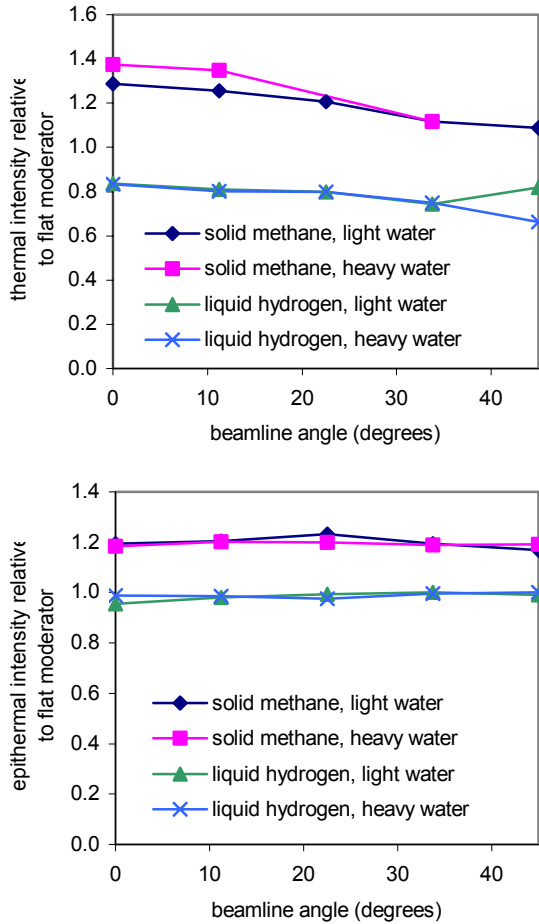


FIG. 6. Thermal (top) and epithermal (bottom) spectral intensities of the grooved moderator relative to the flat moderator for solid methane and liquid hydrogen moderator materials in the coupled moderator position.

Figure 7 shows the thermal and epithermal spectral intensities for the grooved moderator relative to the flat moderator at selected beamline angles other than the normal. The enhancement in thermal neutron intensity for the solid methane moderator decreases from a maximum of about 35% at the normal to the surface to about 10% for a beamline at 45° from the normal but shows an improvement at all angles. The improvement in the epithermal intensity is constant at about 20% for all directions. The liquid hydrogen moderator shows a roughly constant epithermal intensity compared to the flat moderator but a decrease in thermal intensity of about 20% at all angles. We emphasize again that this does not represent optimized performance for either moderator.

Comparing the best performance for the solid methane (grooved) and liquid hydrogen (flat) coupled moderators, we see that the liquid hydrogen provides

more total neutrons and more neutrons in the energy range above 5 meV. The solid methane, however, gives superior performance for a broad range of energies below 5 meV. Further optimization is required before one could make a selection of moderator material for the coupled slab moderator, taking into account the needs of the instruments viewing this moderator.

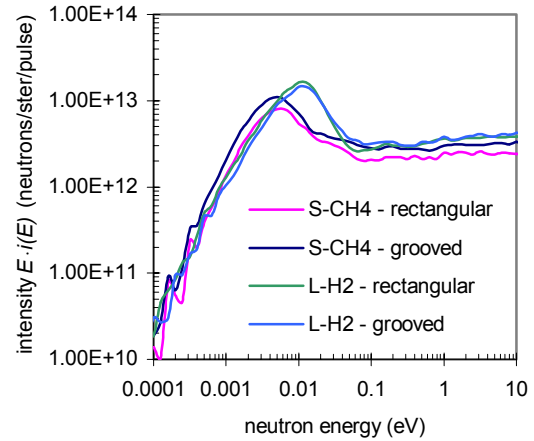


FIG. 7. Neutron spectral intensities for the flat and grooved coupled moderator (direction is normal to the moderator surface).

5. HIGH-ENERGY NEUTRONS

One of the most significant and adventurous design aspects of the LWTS is the use of slab moderators, historically considered awkward due to the contamination of the neutron beams with significant numbers of fast ($0.1 < E_n < 10$ MeV) and high-energy ($E_n > 10$ MeV) neutrons. Because of this contamination, beamlines should not view a slab moderator directly but need to use a curved guide, compact beam bender, or some other filter for fast and high-energy neutrons. The calculations presented here show the variation in the fast and high-energy neutron source term as a function of selected design choices.

Figure 8 shows the variation of the spectral intensity of fast and high-energy neutrons from the slab moderators as a function of angle between the neutron and proton beam directions for the continuous target. This figure clearly shows that there is a “worst case” beamline angle, around 68° from the proton beam direction, where the increased source term and reduced shielding from the target itself are least desirably matched. The highest energy neutrons are still most problematic at the lowest angles relative to

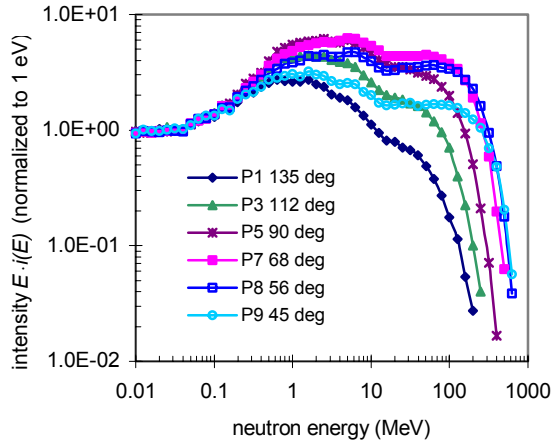


FIG. 8. Fast and high-energy neutron spectra from the slab moderators as a function of beamline angle with respect to the incident proton beam direction.

the proton beam. There is an enormous difference in neutron spectra between beamlines, which may have significant implications regarding the choice of beamline for a given instrument, as some instruments will have restrictions on background and feasible shielding configurations.

Figure 9 shows the fast and high-energy neutron spectra from the front wing moderator, with the high-energy spectrum at 90° from the proton beam direction (i.e., normal to the moderator surface) for the slab moderator shown for comparison. As expected, the fast neutron intensity is significantly smaller for the front wing moderator since the beamlines do not view

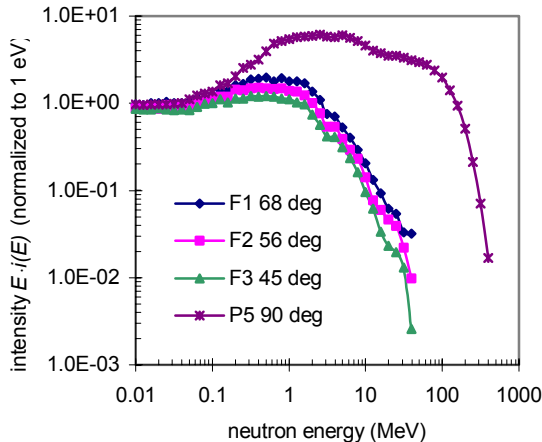


FIG. 9. Fast and high-energy neutron spectra from the front wing moderator, as a function of beamline angle with respect to the incident proton beam direction. The high-energy spectrum at 90° from the slab moderator is shown for comparison.

the target directly, although there is an increase in fast neutrons for beamline angles that approach looking back toward the target.

Our results comparing the LWTS slab to the LWTS front wing moderator are roughly consistent at the highest energies ($E_n \geq 40$ MeV) with measurements carried out some time ago for the German Spallation Neutrons Quelle (SNQ) project.[6] Those measurements indicate a factor of approximately 300-1000 greater fast-neutron intensity from a “slab” moderator configuration than from a “wing” configuration, as shown in Fig. 10. However, the present calculations indicate substantially lower ratios for energies below 20 MeV for the LWTS slab-wing comparison than for the SNQ measurements. Measurements in the LWTS configuration will be needed to resolve this discrepancy. However, the increase in the undesirable neutron component is not tremendously larger for a slab moderator than for a flux-trap moderator, which has been successfully employed at the Lujan Center. The shielding requirements are also, when scaled according to the beam power of LWTS relative to HPTS, reasonably similar to those for the HPTS beamlines. Moreover, experience and measurements at ISIS and SINQ indicate that feasible guide and bender shielding adequately controls the fast neutron component.

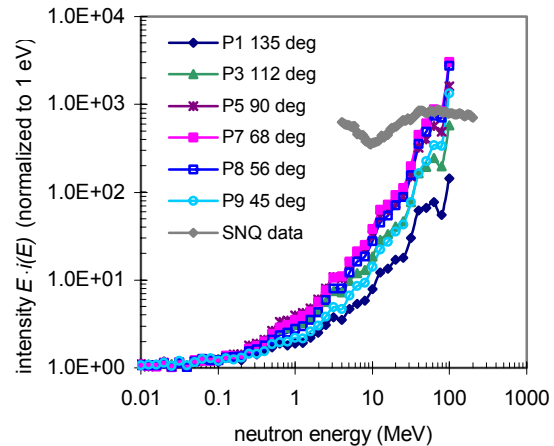


FIG. 10. Ratio of fast and high-energy neutrons for slab moderator beamlines relative to front wing normal. Experimental data from SNQ (slab/wing) [6] are shown for comparison.

6. TARGET HEATING

6.1 Target Energy Deposition

Energy deposition rates in the LWTS target plates were calculated using the MCNPX mesh tally feature. Figure 11 shows the energy deposition rate along the target centerline for the reference LWTS proton beam power of 333 kW. The peak energy deposition is about 253 W/cm^3 and occurs in the second target plate. The energy deposition falls rapidly as the proton beam is depleted due to nuclear interactions, but a small Bragg peak can still be seen at the end of the proton beam range (about 30 cm for 1 GeV incident energy). Approximately 62% of the incident beam power is captured in the target plates and coolant. Figure 12 shows that the energy deposition profile in plates near the upstream end of the target resembles that of the incident proton beam (Fig. 1).

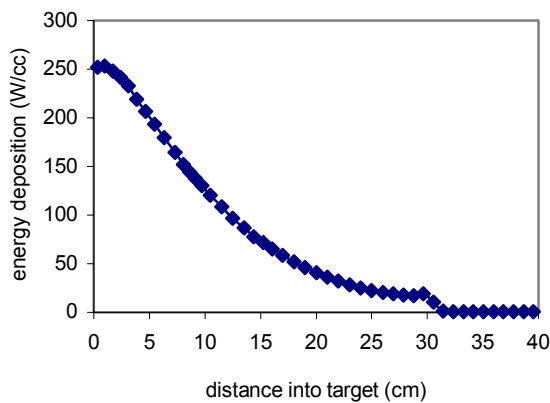


FIG. 11. Energy deposition rate along LWTS target centerline (proton beam power = 333 kW).

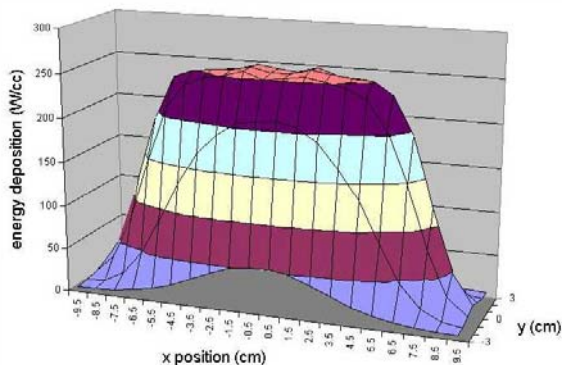


FIG. 12. Energy deposition profile in second LWTS target plate (proton beam power = 333 kW).

6.2 Target Afterheat

Activation determines the afterheat that must be removed from the target in any loss-of-coolant accident (LOCA). Rather than conduct detailed target activation studies, we reviewed activation and afterheat calculations from both the IPNS-Upgrade study [7] and the SNS High-Power Target Station solid-target backup study [8] to determine the afterheat that would result from a tungsten target at the 333 kW proton beam power proposed for the LWTS. We found significant differences between the results of the two studies when compared for constant beam power. The SNS results for afterheat were approximately a factor of two higher for a tantalum target and a factor of four higher for a tungsten target than the corresponding values from the IPNS-Upgrade study. Examination of the buildup (see Fig. 13) and decay rates for the afterheat indicated that the principal nuclides were the same in the two studies, but their creation rates were different. This was due to the use of an activation model in the IPNS-Upgrade calculations that did not contain coolant in the target region (and thus did not accurately account for neutron thermalization in the target) and also neglected radionuclide production due to neutrons under 1 eV.

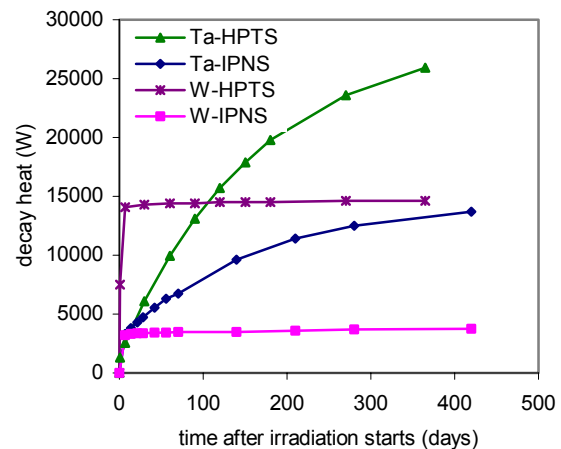


FIG. 13. Target decay heat after shutdown for IPNS-Upgrade and HPTS solid-target backup studies.

In pursuit of an explanation for the discrepancies, we carried out some simple calculations of neutron activation rates in tungsten and tantalum targets using the LWTS target model (including tantalum because it has only one natural stable isotope, and thus analysis of the results is simpler). When comparing the results from the LWTS target (H_2O coolant) with those obtained by counting only activation caused by neutrons above 1 eV in a water-free target, we found that the production of the dominant radionuclide was

underpredicted by a factor of 3.28 in the tungsten target and 1.64 in the tantalum target. It is interesting to note as a result of these calculations that although we usually regard a spallation target as an energetic-particle system, thermal-neutron capture is the dominant mechanism with regard to generation of radionuclides responsible for long-term afterheat.

As a result of these investigations, we chose to adopt the SNS-HPTS solid-target results for afterheat per unit of incident proton beam power. The afterheat for the light-water-cooled LWTS target would be approximately 1.33 times that for the IPNS-Upgrade target. For a heavy water coolant, we expect the afterheat to be somewhat lower because of decreased neutron thermalization in the target region. Since it was concluded in the IPNS-Upgrade study that the target, vessel, and reflector would not melt in a LOCA, and that the consequences of such an accident were tolerable, the same may also hold true for the LWTS. Moreover, the water premoderator layer on the target sides serves as an independent cooling system in the event of a primary coolant LOCA.

CONCLUSIONS

We have devised a highly effective reference conceptual design for the LWTS, which we are still evaluating and optimizing. LWTS will provide distinctly unique capabilities complimentary to the SNS HPTS. The LWTS configuration is closely coupled to instrument requirements through interaction with scientists formulating the science case and instrument suite.

ACKNOWLEDGMENTS

This work was conducted under support from the National Science Foundation Grant DMR-0073038, under the auspices of the US Department of Energy contract W-31-109-ENG-38.

REFERENCES

1. J. M. Carpenter, "Pulsed Spallation Sources for Slow Neutron Scattering," NIM **145**, 91-113 (1977).
2. L. S. Waters, ed., "MCNPX User's Manual, Version 2.1.5," Report TPO-E83-UG-X-00001 (Nov. 14, 1999).
3. R. E. Prael and H. Lichtenstein, "User Guide to LCS: The LAHET Code System," Los Alamos National Laboratory Report LA-UR-89-3014, Revised (Sept. 15, 1989).
4. J. F. Briesemeister, ed., "MCNP – A General Monte Carlo N-Particle Transport Code," Los Alamos National Laboratory Report LA-12625-M, Version 4B (March 1997).
5. E. B. Iverson, B. J. Micklich, and J. M. Carpenter, "Neutronics for the SNS Long Wavelength Target Station," Proceedings of the 15th Meeting of the International Collaboration on Advanced Neutron Sources (Nov. 2000).
6. G. S. Bauer, H. Sebening, J.-E. Vetter, and H. Willax, "Realisierungstudie zur Spallations-Neutronenquelle," technical report, Arbeitsgemeinschaft Spallations-Neutronenquelle, 1981.
7. "IPNS Upgrade: A Feasibility Study," Argonne National Laboratory report ANL-95/13 (April 1995).
8. S. J. Pawel, "Preliminary Materials Recommendation for a Solid Target Back-Up for the SNS," SNS/TSR-0149 (October 29, 1999).